Biomedical Engineering Letters (2019) 9:327–337
https://doi.org/10.1007/s13534-019-00123-x

REVIEW ARTICLE

Advances in the simulation of light–tissue interactions in biomedical engineering

Ilya Krasnikov[1,2] · Alexey Seteikin[1,2] · Bernhard Roth[3,4]

Received: 13 February 2019 / Revised: 15 July 2019 / Accepted: 18 July 2019 / Published online: 25 July 2019

Abstract
Monte Carlo (MC) simulation for light propagation in scattering and absorbing media is the gold standard for studying the interaction of light with biological tissue and has been used for years in a wide variety of cases. The interaction of photons with the medium is simulated based on its optical properties and the original approximation of the scattering phase function. Over the past decade, with the new measurement geometries and recording techniques invented also the corresponding sophisticated methods for the description of the underlying light–tissue interaction taking into account realistic parameters and settings were developed. Applications, such as multiple scattering, optogenetics, optical coherence tomography, Raman spectroscopy, polarimetry and Mueller matrix measurement have emerged and are still constantly improved. Here, we review the advances and recent applications of MC simulation for the active field of the life sciences and the medicine pointing out the new insights enabled by the theoretical concepts.

Keywords Monte Carlo simulation · Biotissue · Light-matter interaction · Scattering and absorbing media

1 Introduction

The same breakthrough in the field of non-operative diagnostic methods as provided by X-ray and computed tomography at the time can now be expected from optical imaging due to the use of non-ionizing radiation and its non-invasiveness [1]. Diffuse reflection spectroscopy (DRS), near infrared spectroscopy (NIRS), diffuse optical tomography (DOT), Raman imaging, fluorescence imaging, optical microscopy, optical coherence tomography (OCT) and photoacoustic (PA) imaging are among the widely used optical methods in biomedicine and their potential is by far not fully explored [2].

✉ Alexey Seteikin
seteikin@mail.ru

1 Amur State University, Ignat'evskoe shosse 21, Blagoveshchensk, Russia 675027

2 Immanuel Kant Baltic Federal University, A. Nevskogo Str. 14, Kaliningrad, Russia 236041

3 Hannover Centre for Optical Technologies, Nienburger Straße 17, 30167 Hannover, Germany

4 Cluster of Excellence PhoenixD, Leibniz University Hannover, Welfengarten 1, 30167 Hannover, Germany

Modeling the propagation of light in a medium is based on the characteristics of absorption and scattering which dominate during the propagation of light in biological tissues. Experimental studies and methods of optical imaging mainly consist in the study of the characteristics of the light which is scattered back to the detector. The photons exit the tissue after either elastic or inelastic scattering in the media. In particular, inelastic scattering carries the molecular signature of the medium and is used, for example, to visualize Raman scattering.

A common approach to simulating the propagation of light in a medium is to use the radiation transfer equation (RTE). Several numerical solutions for the RTE have been proposed, based on suitable approximations, but effective solutions for a heterogeneous medium (tissue) are still a problem [3].

In this review, we consider the advances in the simulation of light–tissue interaction using MC methods, and discuss the main achievements of these methods as well as new applications in biomedical research and engineering. The first three sections are devoted to the basics of the MC approach for modeling the interaction of light and biotissue in the scattering approximation. In the following section, we discuss MC approaches in optical coherence tomography. Then, the modeling of Raman scattering in biotissue is

presented. Finally, the last section is devoted to the applications of MC-based methods to polarimetry and Mueller matrix measurement.

2 Monte Carlo simulation for biotissue modeling

In general, in MC simulations, a large number of photons is propagated through the medium (tissue) under study. In the frame of the current paper, the term photon denotes a package of photons with the same trajectory. Photons can undergo reflection, refraction, absorption, or scattering [4–10]. In these cases, the photons can be reflected, refracted, absorbed or scattered, respectively. The optical properties of the medium such as refractive index (n), absorption coefficient (μ_a), scattering coefficient (μ_s), and scattering anisotropy (g) determine the path traced by the photons in the medium. The absorption coefficient (μ_a) is defined as the probability of photon absorption in a medium per unit (infinitesimal) path length [1].

The MC approach is based on the variation of a statistical weight of the photon package and equivalent to modeling of the propagation of a group of photons along each possible path in the medium. This is achieved by assigning an initial statistical weight W_0 to each photon package. When performing the next propagation step of the photon packet, this weight decreases exponentially due to the random walk of the photons in the multiple scattering and absorbing medium. Finally, when the statistical weight becomes small, a method known as "Russian roulette" gives each photon a chance to continue its path with a weight of n·W, where *n* is a number between 10 and 20. Otherwise, the photon is absorbed completely. This scheme saves computational resources and is designed to balance the incident radiation with absorption and dispersion of radiation in the medium. It has the disadvantage that the length of the photon path in the medium increases unnecessarily, which affects the distribution of photon paths and gives the method some uncertainty. The physical interpretation is also complex and controversial [4].

An MC method, which combines the statistical weight scheme and efficient modeling of the optical path of photons, was implemented in [5, 6]. This approach eliminates the problem of energy conservation that occurs in the "Russian roulette" method and avoids additional calculations for interpretation of the results. The approach is based on modeling a large number of possible trajectories of photon packets from the source to the detector. The simulation of an individual photon packet trajectory consists of a sequence of the following elementary steps: generation of the photon path length, scattering, and refraction (ultimately at the boundary of the medium). The initial and final states of the photons are completely determined by the geometry of the source and detector and the numerical aperture of both.

The medium in which the light propagation is simulated can be defined as an infinite or semi-infinite geometry depending on the simulation needs. For scattering, the polar angle θ and the azimuthal angle φ of the scattered photon depends on the optical properties of the tissue and random value sampling. The angle θ is computed using the Henyey–Greenstein (HG) phase function, which is $p(\cos\theta) = \frac{1-g^2}{2\left(1+g^2-2g\cos\theta\right)^{3/2}}$ and $\varphi = 2\pi\xi$ where ξ is a uniformly distributed random number ξ = [0, 1]. However, the choice of the phase function is not limited to the classical Henyey–Greenstein function. Several authors [7, 8] also introduce a Markov chain solution to model photon multiple scattering through turbid media via anisotropic scattering processes, i.e., Mie scattering. Results show that the proposed Markov chain model agrees well with the commonly used MC simulations (employing the Henyey–Greenstein function) for various media such as ones with non-uniform phase functions or even absorbing media. The proposed Markov chain solution method uses practical phase functions and successfully converts the complex multiple scattering problem into a matrix form. It computes the transmitted/reflected photon angular distributions by relatively simple matrix multiplications.

3 Reduced models for multiple scattering simulation

Beyond using RTE and MC approaches, many studies focused on developing reduced models for multiple scattering processes. Such efforts include the Random Walk theorem [11, 12], empirical predictions [13], and adding-doubling methods [14], among others. These methods typically use simplified analytical expressions to predict the behavior of experimental details, such as the distribution of total transmission, average cosine of scattering, and distance traveled. The use of simple phase functions in these models for describing, for example, the scattering anisotropy g or isotropic scattering also has drawbacks. Such simplifications, although they give reasonable results for some averaged observations, cannot distinguish between similar phase functions, for example, phase functions with the same g, but completely different probability density functions (PDFs) of the photons inside the tissue. Another problem is the limitation when working with anisotropic scattering, absorbing media and/or non-uniform distributions of optical density (OD)/phase functions.

In one example, the Markov chain approximation is used to simulate photon multiple scattering through a turbid slab exhibiting anisotropic scattering [7]. The proposed Markov

chain approximation is considered superior to the MC simulation in handling such problems as it re-formats them into the already mentioned matrix form, allowing feasible input parameter studies and inversion studies for such complex cases. With the matrix form of the Markov chain approximation, one can easily re-write the cost or error function as $Q_{simulation} - Q_{measurement}$ and then minimize this function to infer the desired quantities in a fashion similar to the procedure in [15]. In this context, it is worth noting that there have also been successful experimental investigations in reflected photon angular distribution measurements confirming the simulations [16].

4 Beam spread function approach for optogenetics

In recent years, optogenetics has become a central research area in neuroscience. For example, estimating the transmission of visible light through brain tissue is of crucial importance for controlling the activation levels of neurons in different depths, designing optical systems, or estimating and avoiding lesions from excessive power density exposure [17]. Two modified approaches for modeling the distributions of light emanating from a multimode fiber and propagating through scattering tissue are introduced and studied, using both realistic numerical MC simulations and an analytical approach based on the beam spread function (BSF) concept (Fig. 1). Good agreement of the new methods' predictions both with recently published data and with measurements in mouse brain cortical slices is demonstrated. In the latter case, results yield a new cortical scattering length estimate of ~47 μm at λ = 473 nm, significantly shorter than ordinarily assumed in other optogenetic applications.

These results put forward the beam spread function (BSF) method as a viable analytic approach to better understanding of light propagation and interactions in optogenetics and related fields, while using the Kubelka–Munk (K–M) model based on one parameter only, the scattering coefficient μ_s, appears inadequate. The K–M model has a particularly simple solution in the case of semi-infinite samples. All the geometric features of the inhomogeneous sample are combined into a single semi-empirical parameter to take into account the internal scattering processes, i.e. the scattering coefficient μ_s. Generally, the

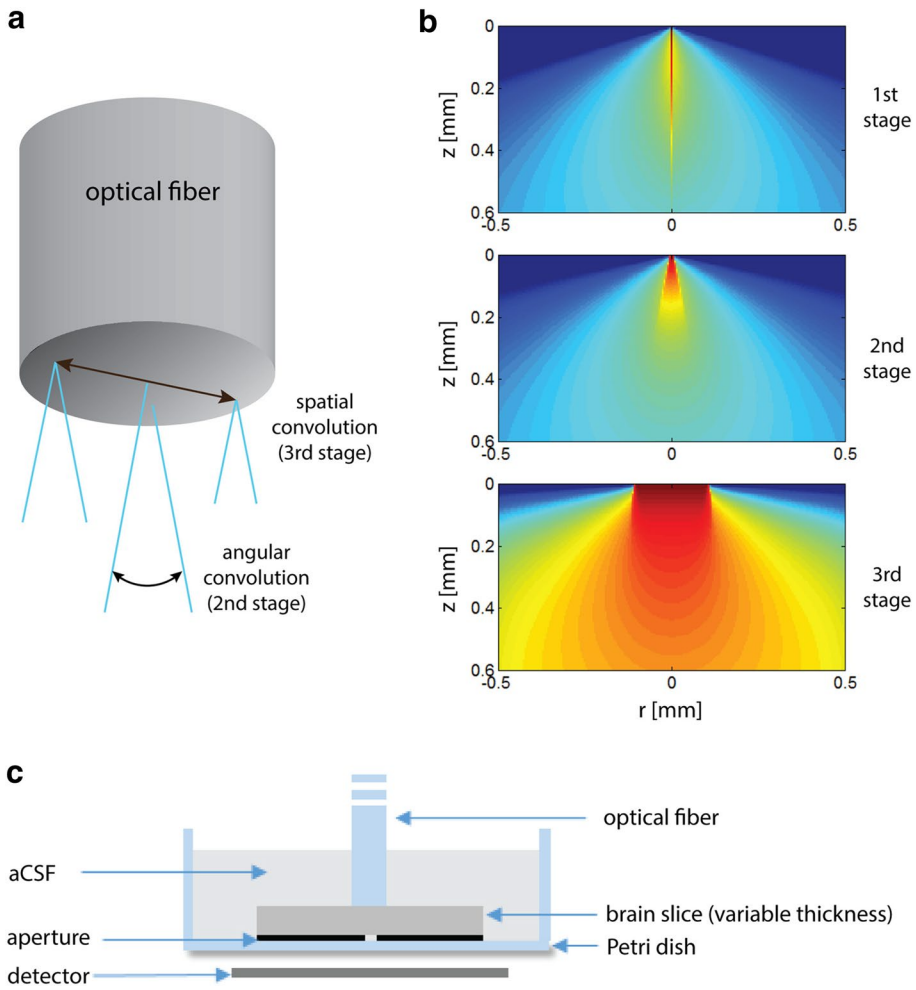

Fig. 1 **a** Simulation key points: in the 1st stage the 3D pencil-beam response is calculated, in the 2nd stage the angular convolution of the pencil beam response, and in the 3rd stage the spatial convolution with the fiber tip area. **b** Simulation outcomes for the three simulation steps. All figures are given in log scale. **c** Schematic of the experimental setup. Reproduced from [17], with permission

scattering coefficient μ_s depends on the particle size and the refractive index of the sample, while in the K–M model it is assumed to be constant. In fact, the scattering coefficient changes slowly with wavelength. More importantly, it changes significantly with packing density. According to the authors, the BSF can be used both to calculate the distribution of light in the brain tissue and to estimate optical parameters from measured attenuation curves [17].

The BSF method [18] approximates the distribution of light in strongly scattering media, taking into account the effects of higher order photons propagating via several paths of different lengths. It also allows to calculate time dispersion of the light intensity. In this approach, the Green's function is an analytical approximation for the unidirectional propagation of a pulsed source in a turbid medium. The simulation time of the BSF approach of a pencil beam is considerably smaller than for the MC approach at comparable accuracy. The accelerated gradient search method was implemented by Beck and Teboulle [19] to find the scattering coefficient and anisotropy factor [20, 21].

In order to describe the above optogenetics problem with MC simulations several aspects need to be addressed. At the heart of the MC method is the assumption that the medium is homogeneous. Therefore, one of the problems, among others, is the assumption of homogeneity of the brain tissue. However, the cortical layers of the brain have different cytological properties and necessarily different optical parameters. They can be obtained by fitting the attenuation curve in parts, using histologically determined layers Azimipour et al. [22].

As mentioned above, in vivo methods in optogenetics are widespread. However, to date, the effects of direct exposure of brain tissue to light have not been studied in detail and require additional research. Special attention is attracted by the effect of heat release and heat transfer in biological tissues induced by prolonged optical stimulation, as discussed in [23]. In the same work it is shown that high-intensity light delivered through an optical fiber can locally increase the rate of excitation of neurons, taking into account the properties of the environment. Therefore, the creation of a dosimetry model to predict an increase in temperature during optogenetic stimulation is a very important task. A realistic model is required that simulates the propagation of light and heat during optogenetic experiments which is currently still under study.

5 Monte Carlo approaches in optical coherence tomography

Optical coherence tomography (OCT) is a non-invasive technique which enables fast imaging with high resolution down to the few micrometer range. For the needs of modern medicine, such high-speed imaging techniques are widely required. This approach is advanced by recent developments in the field of tunable laser technologies and miniaturization concepts [24–27]. Simulations were developed along with the technology and meanwhile even take into account additional parameters of the setup such as realistic geometric and interferometric conditions as well as requirements for detection [28]. Most numerical approaches so far are based on the MC method. Smithies and co-workers [29] developed an MC OCT model taking a geometrical implementation of the OCT probe with low-coherence interferometric detection into account. It was found that OCT, in general, detects only minimally scattered photons. Alerstam and co-workers [30] described a highly optimized MC code package for simulating light transport developed on NVIDIA graphics processing units (GPUs). It is built for general-purpose computing Fermi GPU micro architecture.

In [31], a simple and effective model based on the MC method for simulating OCT signals, scattering coefficients and the effect of multiple photon scattering with increasing concentration of scatterers is presented. It is important to note, that although the model accurately estimates the optical parameters of sample, it does not require the inclusion of more complex effects, such as dependent and multiple scattering. Instead, a certain weight function is introduced that describes the different orders of multiple scattering events.

Practice shows that the main problem in quantitative OCT measurements is the linear dependence of the scattering coefficient μ_s on the concentration of diffusers, in the case of weakly scattering homogeneous media. In the case of strong scattering, the dependence becomes nonlinear and, therefore, more complex. The model developed in [31] is capable of accurately predicting this non-linearity and has the potential to be extended to OCT studies of biological tissues and the corresponding determination of optical properties in the future.

Chumakov et al. [32] report on the investigation of the vector method for modeling of the propagation of polarized electromagnetic radiation with small coherence length for application in polarization OCT. The MC method was used to model the coherent effects of multiple scattering, and a comparison was made with an iterative approach to solving the Bethe–Salpeter equation [33]. Multiple scattering was determined as the sum of partial contributions corresponding to each registered photon, taking into account the function of time coherence

$$I_{OCT}(\tau) = \sum_{i=1}^{N_{ph}} W_i \cos\left(\frac{2\pi}{\lambda}\Delta L_i\right) exp\left[-4lg2\left(\frac{\Delta L_i}{l_c}\right)^2\right], \quad (1)$$

where W_i is the statistical weight of the photon, ΔL_i the optical path difference for this photon and a photon in the

reference arm, λ the wavelength of a radiation source in the medium, and N_{ph} the sampling power. The expression describes the time delay of scattered radiation with respect to the reference signal. After time averaging, it gives rise to an additional stochastic background in the form of speckles.

In the proposed MC vector model, an important parameter is the polarization vector P of the radiation, which can measure changes in the electromagnetic field when propagating through a medium. The simplicity of the calculations of the polarization vector at the output of the medium with the co-polarized and cross-polarized components of the scattered field is an advantage of the vector approach compared with methods based on the Mueller matrix, see below.

6 Raman spectroscopic simulation based on efficient Monte Carlo concepts

Raman spectroscopy has advantages compared with other spectroscopic methods widely used in the life sciences, for example, approaches based on fluorescence detection. First, Raman signals do not bleach and secondly, Raman lines/bands are spectrally narrow, which improves discrimination of signals in complex media [34]. Research on the use of Raman spectroscopy for biological tissues is maturing only slowly, and at this stage, quantitative analysis of spectroscopic combination signals in biological tissue is difficult. Typically, biological samples contain a variety of molecular species, and, in addition, measurements are altered by the attenuation of the combinational signal through self-absorption in the tissue. Realistic numerical simulation of the process of Raman scattering can help in carrying out a quantitative analysis of Raman spectra, which is highly desirable. However, approaches are still scarce and often take a long time. Numerical simulation of Raman scattering consists of two stages: (1) the calculation of the photon fluence at each point of the medium and (2) the subsequent generation of the corresponding number of Raman scattered photons at each point.

To effectively simulate Raman scattering in turbid media irradiated with light, two different methods have recently been published [35]. Both approaches use the MC method to simulate the Raman process. In the first approach, the direct method, it is assumed that the absorption coefficient $\mu_a(\lambda_{Raman})$ and the coefficient of Raman scattering $\mu_s(\lambda_{Raman})$ are constant throughout the sample for a given wavelength of the Raman photon λ_{Raman}. With the photon propagating into the medium, with some probability P_{Raman}, re-emission of a new photon, the Raman scattered photon can occur (Fig. 2). The value of P_{Raman} is constant for each step, since the scattering length, i.e., the photon path between the individual scattering events, is also assumed to be constant. A Raman photon can propagate through a medium with a random direction for the next step, which corresponds to isotropic scattering. The optical properties of the medium at a specific wavelength of the Raman scattered light λ_{Raman} are used to propagate the photons in the next step. To generate a reasonable amount of combinational photons in this one-pass approach, the estimated value of P_{Raman} is chosen quite (unphysically) large ($P_{Raman}=0.01$). Realistically, P_{Raman} needs to be set five to ten orders of magnitude smaller than the Rayleigh (elastic) scattering probability. However, according to the work of Everall et al. [36] the assumption employed in [35] is well justified.

The second approach, the so-called two-step method, creates sufficient Raman scattered photons without increasing P_{Raman} or the number of incident photons. The first step here is identical to the MC code in [14]. It simulates the propagation of the incident photons through the sample, which results in a photon deposition distribution of the excitation (parent) photons $A_{ex}(r, z)$. In combination with the absorption coefficient μ_a this determines the spatial distribution of the excitation photons $\Phi_{ex}(r, z)$ within the sample. In the second step, Raman scattered photons are launched from each point where "parent" photons were absorbed with isotropically distributed directions and a weight of

$$W_{Raman} = \Phi_{ex}(r, z) \cdot \mu_{Raman}, \tag{2}$$

where r represents the radial coordinate in the isotropic case. The Raman coefficient μ_{Raman} is comparable with the Raman

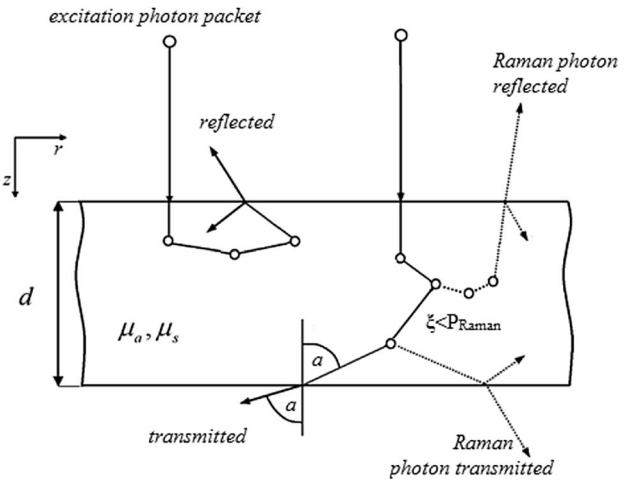

Fig. 2 General scheme of the Raman MC simulation model used for both the direct and the two-step method. In the direct approach, the initial photon (package) moves in a medium and can be Raman scattered at any moment. In the two-step approach, the propagation of Rayleigh photons is modeled first. At each step (circles) where absorption occurs some of the photons from the packet are terminated and Raman photons are launched and propagated as well. Solid lines show the trajectories of elastically scattered photons, the trajectories of Raman scattered photons are represented by dashed lines. While z denotes the depth of the sample, r denotes the distance from the center of illumination, that is, the radial coordinate. Reproduced with permission from [35], [OSA Publishing]

probability P_{Raman} of the direct method. If just a single photon at each unit volume of the sample was created, this would not lead to a large enough number of photons required to obtain suitable statistics in the simulations. Therefore, the described algorithm creates any desired number of photons within the sample. The distribution of the photons starting in the second step of the process is similar to the excitation photon distribution Φ_{ex}. In other words, $\Phi_{ex}(r, z)$ is scaled with the number of photons intended to be allocated in the simulation grid which is determined by $A_{ex}(r, z)$.

Furthermore, in the work of Reble et al. a method that could correct Raman signals for the influence of optical properties in a large parameter range without a priori assumptions of the absorption and scattering properties was investigated [37]. Possible correction functions were employed to correct the Raman signals for the influence of the tissue optical properties.

Everall et al. [36] used MC simulations to study the time-resolved migration of Raman and Tyndall photons, i.e. photons scattered by particles with sizes on the order of the wavelength of the light, in opaque samples with isotropic and direct scattering. A suitably large value of the probability of Raman scattering ($P_{Raman} = 0.01$) was used to model a sufficient number of photons, for statistical reasons. So far, most models are based on a two-step approach for Raman modeling, similar to fluorescence modeling, and only a few papers directly implement Raman photon scattering.

In [35] a comparison between the two simulation methods, the direct method and the two-step method, was performed. For both cases, the spatial distribution of the absorbed light for Raman scattering in a medium that is illuminated with a laser beam of finite beam dimension was calculated. The simulations are realized using the NVidia CUDA technology to increase the calculation speed and are optimized for high-precision.

Both methods have advantages in different parameter regimes, and, as the comparative study shows, the results are generally in good agreement. Furthermore, both approaches work with acceptable photon statistics. However, the two-step method usually leads to a smoother photon distribution or absorption profile, because the launch of new Raman scattered photons in the second step provides a good statistical representation of stochastic events. The implementation of the two-step method is clearer and simpler and does not require major modification of the source code MC or an unrealistically large number of P_{Raman}. The direct method, on the other hand, has the advantage that its procedure is closer to the actual processes in a laser-illuminated medium that is Raman active.

One of the main applications of Raman spectroscopy is to measure the chemical composition of a sample, which can then be used to extract static or dynamic biological information from that sample. Increasing the accuracy of Raman spectroscopy models in scattering media, such as biological tissue, requires more precisely defined optical parameters of the medium, accurate detector parameters and the sample geometry to be included in the model. As an example, two cases were studied that represent some of the most common configurations in Raman spectroscopic studies: a confocal Raman setup and a fiber-optic probe setup. In addition, with regard to the samples under study, the model effectively simulates Raman signals for different single and multilayer samples with arbitrary geometry, including both focused and collimated lasers for excitation as well as different values of the numerical aperture NA of the optics and the radius of the exciting beam, respectively [38].

For convenience, the model introduces the concept of a cross section for Raman scattering or, alternatively, the probability of a Raman scattering event, μ_{Raman}, similar to the cross section for elastic scattering [21, 35, 37, 39, 40]. The advantage of using this parameter lies in the fact that for each simulation step it represents the probability that the photon in question is re-emitted as a Raman photon. When calculating the photon distribution the two-step model is thus more beneficial [35]. Given the fact that the process of Raman scattering is very weak, this approach greatly accelerates the simulation of Raman scattering, which is mandatory for modeling complex environments and geometries [35, 41–43].

When designing a Raman setup for conducting experiments, the signal is usually obtained in reflection mode. However, as shown by the simulations, large values of the scattering or absorption coefficients of the samples lead to a decrease in the intensity of the Raman signals on the surface [38]. In addition, the existence of boundaries between individual layers of a multilayer medium where each layer exhibits different optical properties has a significant effect on the distribution of the optical radiation inside the sample and the detected Raman signal outside the sample. Differences in absorption and scattering as function of wavelength lead to a change in the fluence of the Raman photons and the detected Raman intensity. This fact is usually crucial when Raman spectroscopy is to be used as a quantitative measurement tool. Thus, incorporating self-absorption of the Raman signal in biological media potentially allows for quantitative measurements in the future [38, 44].

In another study, an attempt to model Raman scattering of normal human skin in the near infrared (NIR) wavelength range was addressed [45]. An eight-layer skin model was built with transport parameters adapted from a number of publications. The calculation of the 785 nm excitation light distribution inside the model medium was performed directly with the MC code from Wang and Jacques [4]. The code was modified to simulate the Raman escape process from the medium. It was assumed that the exit process of a Raman photon is similar to the exit of a fluorescence photon

from inside the tissue. Therefore, the same modeling procedures that were developed in fluorescence modeling [46–49], were used to simulate Raman scattering, which consist of the following steps:

1. Calculate the excitation light distribution inside the model skin.
2. Calculate the escape functions for different wavelengths and at different depths.
3. Calculate the Raman detection efficiency as a function of wavelength for different skin layers.
4. Calculate the simulated Raman spectra.

Raman spectra of ex vivo normal skin tissue sections were measured to quantify the different intrinsic micro-spectral properties of the skin layers [45]. The reconstructed skin Raman spectrum was compared with clinically measured in vivo skin spectra to verify the utility of the modelling approach, see Fig. 3. To obtain the reconstructed Raman spectra, a convolution of the intrinsic spectra with the MC simulation results of the excitation light distribution and the Raman photon escape efficiency was performed. The simulations suggest that the majority of the measured in vivo skin Raman signals come from the dermis (70%) and the epidermis (28%). The stratum corneum, although very thin, still has non-negligible contributions (1.3%) due to its near-to-surface location which facilitates escape of the Raman photons. The contribution of the subcutaneous layers is also not negligible (1.1%) due to its much higher Raman scattering efficiency compared to other tissue layers (4–5 times higher than those of the epidermis/dermis), although it is located deep inside the skin. In essence, an overall good agreement between simulated and measured data was obtained.

7 Polarimetry and Mueller matrix measurement

All necessary information for analyzing the polarization changing properties of a biological sample is contained in the Mueller matrix. It can be calculated from images of a sample taken with different polarization states of the illuminating and the observed light. Using the Mueller matrix it is then possible to calculate the Stokes vector of the outgoing light $\left(\vec{S}_o\right)$ after interaction with a medium for incoming light with Stokes vector $(\vec{S}_i)$ according to $(\vec{S}_o) = \mathrm{M}_{\mathrm{MM}} \cdot (\vec{S}_i)$. Thus, the potential opens up that Mueller matrix imaging polarimetry becomes a new and possibly very efficient technique for the optical biopsy and cancer staging. Usually, this is currently tested by measuring on ex vivo samples of human tissue, as in vivo measurements are often not feasible. Multispectral polarimetric images performed, for example, on human colon and uterine cervix samples reveal an enhanced contrast between healthy and cancerous zones compared to the unpolarized intensity images [50].

In this approach, the MC method was applied to simulate the Mueller matrices of tissue samples and also for better understanding of the physical origin of the observed polarimetric contrast [51–53]. Such an approach requires the use of multi-layered optical tissue sample models. Thus, the tissue is treated as a multi-layer medium where each layer is characterized by the anisotropy factor g, the absorption coefficient μ_a, the scattering coefficient μ_s, and the refractive index n. Optical properties are assumed constant for each layer. Through repeated modelling experiments, it was found that the optical properties of different layers and the corresponding layer boundaries strongly influence the distribution

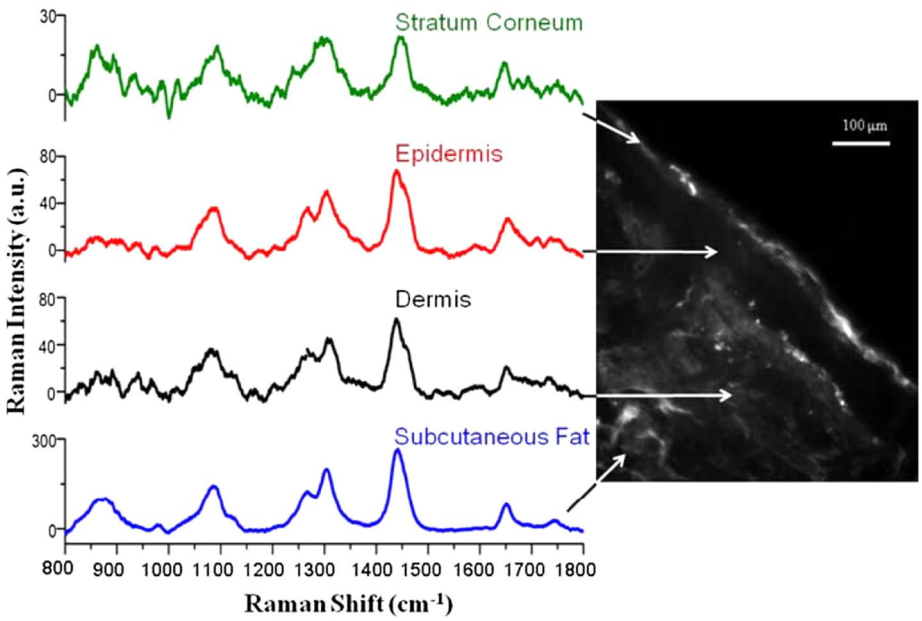

Fig. 3 (Left) intrinsic Raman spectra measured from different layers of an unstained excised normal skin sample. (Right) NIR auto-fluorescence image of the skin section showing the measurement locations. Reproduced from [49], with permission

of photons in the medium. For sufficiently large scattering and absorption coefficients, the largest number of photons is scattered or absorbed in the upper layers of the tissue [38]. The detailed analysis of the simulation results and experimental studies show that objects that are sufficiently small compared to the wavelength of light are the main sources of back-scattering events in the tissue [50].

The analysis of the measured Mueller matrix of a sample begins with the decomposition of the final matrix into a product of elementary matrices with known polarimetric properties. Such a decomposition can be obtained by various approaches. In some studies, the Lu–Chipman decomposition was applied [54, 55], where the Mueller matrix M of image samples is decomposed pixel-wise into the product of three matrices:

$$M = M_{\Delta} M_R M_D, \tag{3}$$

where M_{Δ}, M_R, M_D are the matrices of a depolarizer, a retarder and a diattenuator, respectively. This can then be used for numerical analysis of the measured samples in terms of the effective scalar birefringence, orientation of the optical axis and depolarization. The general trend for the wavelength-dependent depolarization and scalar birefringence shows that Mueller matrix polarimetry is capable to differentiate between healthy and diseased tissues [50].

In more detail, it was shown on ex vivo measurements of excised colon samples that tumor areas are less depolarizing than healthy areas at the early stage of cancer. Also, depolarization is always higher for circular polarization of the light incident to the sample compared to linear polarization, both for healthy and cancerous tissue [50, 52].

For comparison with the measurements, the Mueller matrix images of human colon tissue were simulated by MC techniques using the above mentioned multi-layer tissue models with different scattering and absorption coefficients of the individual layers, see Fig. 4. Through the comparison with experimental data it was demonstrated that the measured values of depolarization for both circular and linear polarized incident light and for healthy and anomalous tissues can be qualitatively reproduced only when small (compared to wavelength of the light) scatterers are incorporated into the optical model [50].

Finally, Doronin et al. [56], in an effort to develop a unified MC code for biomedical optics and biophotonics applications, presented an approach for modeling of coherent polarized light propagation in highly scattering turbid media. In this approach, the temporal coherence of the light, linear and circular polarization, interference, and the helicity flip of circularly polarized light due to reflection at the medium boundary and/or back-scattering are taken into account. A Jones-based formalism was adapted to handle linear or

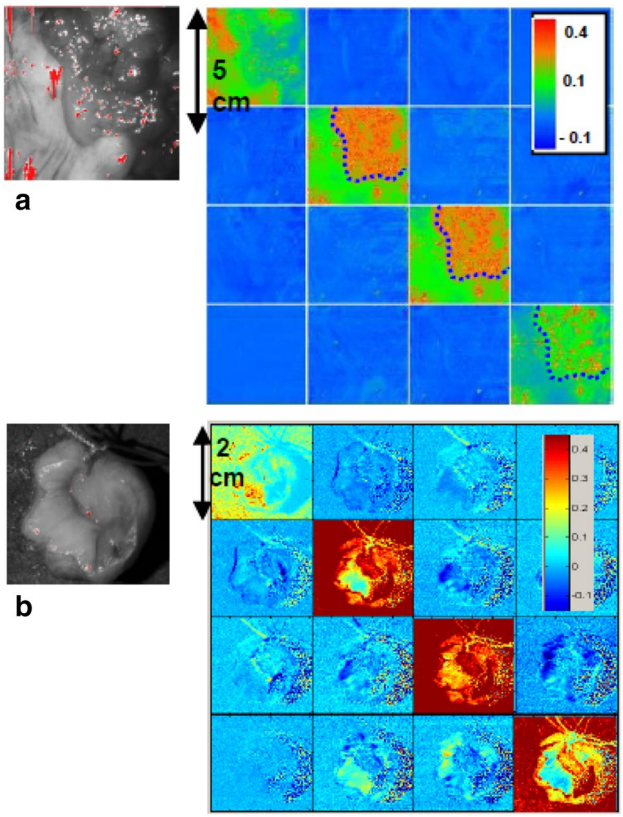

Fig. 4 Intensity and Mueller matrix images of excised samples investigated using **a** optical radiation at 600 nm for human colon cancerous polyp and **b** at 500 nm for cancerous uterine cervix. Reproduced from [50], with permission

circular polarization of coherent light traveling through a random turbid medium. The propagation of linear polarized light in a scattering medium is modeled in analogy to the iterative procedure of the solution of the Bethe–Salpeter equation [57]. Reported results and analytical solutions by Milne and the results of alternative modeling [58–61] are in good agreement for both linearly and circularly polarized light. The approach also provides a certain flexibility to account for the optical properties of the medium and the light source and is realized as a part of a user-friendly and fast GPU calculation platform [56].

In [62], a theoretical model of the scattering of polarized radiation was developed and simulation of OCT images was performed. Using an innovative interpretation of the MC simulation and a complex skin model, the authors obtained expressions for the contribution of the co-polarized and cross-polarized radiation components to the OCT image of the sample (Fig. 5). An further aspect in related work is the possibility of modeling light propagation with and without taking speckle effects into account, which quantitatively demonstrates the influence of these

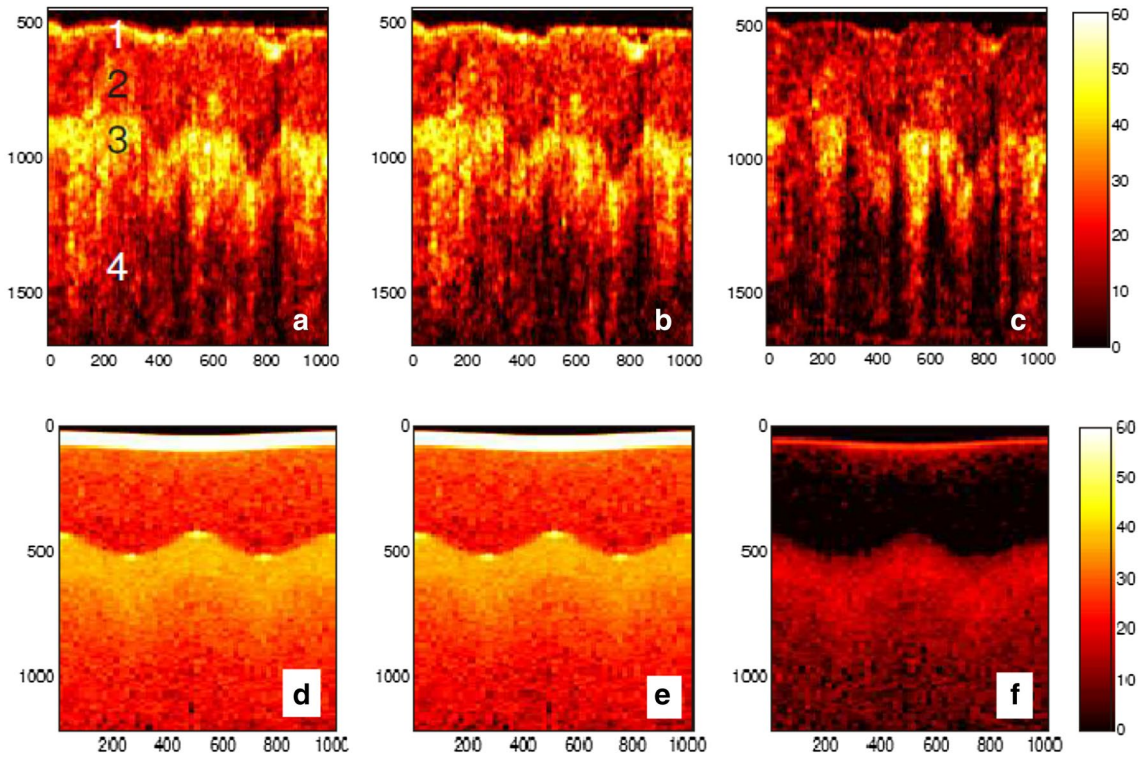

Fig. 5 **a–c** Experimental 2D OCT images of human skin in vivo obtained for non-, co- and cross-polarized modes, respectively. Upper stratum corneum (1), lower stratum corneum (2), epidermis (3) and dermis (4) are clearly distinguished in the OCT images. **d–f** Simulated 2D OCT images obtained for non-, co- and cross-polarized modes, respectively. The coherence length of the low-coherent light source is 15 µm. Reproduced with permission from Ref. [62], [OSA]

effects in the formation of, for example, OCT images [63, 64]. The capabilities of the developed code are illustrated by the good correlation with OCT images of human skin in vivo, compare also [65].

In a continuation of previous research, in [66] using Monte-Carlo simulation with GPU CUDA the propagation of cylindrical vector beams (CVB) in turbid tissue-like scattering media was explored in comparison with conventional Gaussian laser beams. The authors also pioneered the application of MC for imitation of the propagation of vector light beams in turbid media. The results are compared with the results obtained by experiment and show good agreement both quantitatively and qualitatively. The model developed by the authors includes the coherent properties of light, taking into account the effect of total reflection and refraction at the boundary of the medium. A distinct aspect of the model is the fact that it also takes into account the mutual interference of the polarization components of the CVB wavefront due to scattering in the medium. It was shown that the degree of contrast achieved when using CVBs is at least twice as large compared to conventional linearly polarized Gaussian beams after propagation in a turbid tissue-like scattering medium.

8 Summary

The MC based simulation of light propagation in biological tissue has emerged to an important tool for understanding the subtleties of the light–matter interaction in complex media relevant to the fields of medicine and the life sciences, for example. Apart from efficient simulation algorithms accurate modeling is the key for the recent advances in the field. New insights obtained from the simulations serve as valuable input for the design of novel instruments based on non-invasive, optical principles or facilitate the interpretation of measured data obtained from biological samples. The simulation methods presented in this review are mainly focused on biomedical optical imaging and spectroscopy [67]. However, they will likely influence further fields of application in the near future. Consequently, intense research is currently under way to develop more comprehensive and at the same time efficient simulation tools taking into account all aspects of the system itself as well as incorporating all relevant environmental influences. Also, the trend points towards the use of anatomically more realistic geometries and the development of more user-friendly simulation tools. As the field is already undergoing the translation from basic research to practical applications, for example,

in clinical environments or in the field, a large variety of optical systems with enhanced functionality are expected to evolve in the mid and long term. Further benefit will be generated by the ever increasing computing power available and artificial intelligence concepts such as machine learning and deep learning concepts which will likely also advance modeling and simulations as well as data analysis.

Funding The State task of the Ministry of Education and Science of the Russian Federation (Project # 3.5022.3017/8.9). B.R. acknowledges funding by the Deutsche Forschungsgemeinschaft (DFG, German Research Foundation) under Germany's Excellence Strategy within the Cluster of Excellence PhoenixD (EXC 2122).

Compliance with ethical standards

Conflict of interest The authors have no conflicts of interest to declare.

Ethical approval This article does not contain studies with human participants or animals.

References

1. Wang LV, Wu H-I. Biomedical optics: principles and imaging. Hoboken, NJ: Wiley; 2009.
2. Yun SH, Kwok SJ. Light in diagnosis, therapy and surgery. Nat Biomed Eng. 2017;1:0008.
3. Liu K, et al. Evaluation of the simplified spherical harmonics approximation in bioluminescence tomography through heterogeneous mouse models. Opt Express. 2010;18:20988–1002.
4. Chumakov, et al. Influence of refractive index matching on the photon diffuse reflectance. Phys Med Biol. 2002;47(23):4271–85.
5. Meglinsky IV, Matcher SJ. Modelling the sampling volume for skin blood oxygenation measurements. Med Biol Eng Comput. 2001;39:44–50.
6. Meglinsky IV, Matcher SJ. Analysis of the spatial distribution of the detector sensitivity in a multilayer randomly inhomogeneous medium with strong light scattering and absorption by the Monte Carlo method. Opt Spectrosc. 2001;91:654–9.
7. Lin Y, Northrop WF, Li X. Markov chain solution of photon multiple scattering through turbid slabs. Opt Express. 2016;24(23):26942–7.
8. Xu F, Davis AB, Sanghavi SV, Martonchik JV, Diner DJ. Linearization of Markov chain formalism for vector radiative transfer in a plane-parallel atmosphere/surface system. Appl Opt. 2012;51(16):3491–507.
9. Wang L, Jacques SL. Animated simulation of light transport in tissues. Proc SPIE. 1994;2134:2134A.
10. Periyasamy V, Pramanik M. Advances in Monte Carlo simulation for light propagation in tissue. IEEE Rev Biomed Eng. 2017;10:122–35.
11. Gandjbakhche AH, Weiss GH, Bonner RF, Nossal R. Photon path-length distributions for transmission through optically turbid slabs. Phys Rev E Stat Phys Plasmas Fluids Relat Interdiscip Top. 1993;48(2):810–8.
12. Li X, Ma L. Scaling law for photon transmission through optically turbid slabs based on random walk theory. Appl Sci. 2012;2(4):160–5.
13. Sun X, Li X, Ma L. A closed-form method for calculating the angular distribution of multiply scattered photons through isotropic turbid slabs. Opt Express. 2011;19(24):23932–7.
14. Welch AJ, Van Gemert MJ. Optical-thermal response of laser-irradiated tissue, vol. 2. Berlin: Springer; 2011.
15. Ma L, Li X, Sanders ST, Caswell AW, Roy S, Plemmons DH, Gord JR. 50-kHz-rate 2D imaging of temperature and H_2O concentration at the exhaust plane of a J85 engine using hyperspectral tomography. Opt Express. 2013;21(1):1152–62.
16. Wax A, Yang C, Backman V, Kalashnikov M, Dasari RR, Feld MS. Determination of particle size by using the angular distribution of backscattered light as measured with low-coherence interferometry. J Opt Soc Am A. 2002;19(4):737–44.
17. Yona G, Meitav N, Kahn I, Shoham S. Realistic numerical and analytical modeling of light scattering in brain tissue for optogenetic applications. eNeuro. 2016;3(1):1–9.
18. McLean JW, Freeman JD, Walker RE. Beam spread function with time dispersion. Appl Opt. 1998;37:4701–11.
19. Beck A, Teboulle M. A fast iterative shrinkage-thresholding algorithm for linear inverse problems. SIAM J Imaging Sci. 2009;2:183–202.
20. Aravanis AM, Wang LP, Zhang F, Meltzer LA, Mogri MZ, Schneider MB, Deisseroth K. An optical neural interface: in vivo control of rodent motor cortex with integrated fiberoptic and optogenetic technology. J Neural Eng. 2007;4:S143–56.
21. Zhu C, Liu Q. Review of Monte Carlo modeling of light transport in tissues. J Biomed Opt. 2013;18:50902.
22. Azimipour M, Baumgartner R, Liu Y, Jacques SL, Eliceiri K, Pashaie R. Extraction of optical properties and prediction of light distribution in rat brain tissue. J Biomed Opt. 2014;19:075001.
23. Stujenske JM, Spellman T, Gordon JA. Modeling the spatiotemporal dynamics of light and heat propagation for in vivo optogenetics. Cell Rep. 2015;12:525–34.
24. Zhang A, Zhang Q, Chen C-L, Wang RK. Methods and algorithms for optical coherence tomography-based angiography: a review and comparison. J Biomed Opt. 2015;20:100901.
25. Drexler W, Liu M, Kumar A, Kamali T, Unterhuber A, Leitgeb RA. Optical coherence tomography today: speed, contrast, and multimodality. J Biomed Opt. 2014;19:71412.
26. Wieser W, Draxinger W, Klein T, Karpf S, Pfeiffer T, Huber R. High definition live 3D-OCT in vivo: design and evaluation of a 4D OCT engine with 1 GVoxel/s. Biomed Opt Express. 2014;5:2963.
27. Kim J, Brown W, Maher JR, Levinson H, Wax A. Functional optical coherence tomography: principles and progress. Phys Med Biol. 2015;60:211–48.
28. Thrane L. Optical coherence tomography: modeling and applications. Rosklide: Risø National Laboratory; 2001.
29. Smithies DJ, Lindmo T, Chen Z, Nelson JS, Milner TE. Signal attenuation and localization in optical coherence tomography studied by Monte Carlo simulation. Phys Med Biol. 1998;43:3025.
30. Alerstam E, Yip Lo WC, Han TD, Rose J, Andersson-Engels S, Lilge L. Next-generation acceleration and code optimization for light transport in turbid media using GPUs. Biomed Opt Express. 2010;1:658.
31. Varkentin A, Otte M, Meinhardt-Wollweber M, Rahlves M, Mazurenka M, Morgner U, Roth B. Simple model to simulate OCT-depth signal in weakly and strongly scattering homogeneous media. J Opt. 2016;18(125302):1–10.
32. Churmakov Yu, Kuz'min V, Meglinski I. Application of the vector Monte-Carlo method in polarisation optical coherence tomography. Quantum Electron. 2006;36:1009–15.
33. Kuz'min VL, Meglinskii IV. Numerical simulation of coherent backscattering and temporal intensity correlations in random media. Quantum Electron. 2006;36(11):990–1002.

34. Shih W-C, Bechtel KL, Feld MS. Intrinsic Raman spectroscopy for quantitative biological spectroscopy. Part I: theory and simulations. Opt Express. 2008;16:12726–36.
35. Krasnikov I, Suhr C, Seteikin A, Roth B, Meinhardt-Wollweber M. Two efficient approaches for modeling of Raman scattering in homogeneous turbid media. J Opt Soc Am A. 2016;33(3):426–33.
36. Everall N, Hahn T, Matousek P, Parker AW, Towrie M. Photon migration in Raman spectroscopy. Appl Spectrosc. 2004;58:591–7.
37. Reble C, Gersonde I, Andree S, Eichler HJ, Helfmann J. Quantitative Raman spectroscopy in turbid media. J Biomed Opt. 2010;15:037016.
38. Krasnikov I, Seteikin A, Kniggendorf A-K, Roth B, Meinhardt-Wollweber M. Simulation of Raman scattering for realistic measurement scenarios including detector parameters and sampling volume. J Opt Soc Am A Opt Image Sci Vis. 2017;34(12):2138–44.
39. Meglinski I, Doronin AV. Monte Carlo modeling of photon migration for the needs of biomedical optics and biophotonics. In: Tuchin VV, Wang RK, editors. Advanced biophotonics: tissue optical sectioning. London: Taylor & Francis; 2012.
40. Tuchin V, editor. Handbook of optical biomedical diagnostics, vol. PM107. Washington: SPIE Press; 2002.
41. Lukic A, Dochow S, Bae H, Matz G, Latka I, Messerschmidt B, Schmitt M, Popp J. Endoscopic fiber probe for nonlinear spectroscopic imaging. Optica. 2017;4(5):496–501.
42. Varkentin A, Mazurenka M, Blumenröther E, Behrendt L, Emmert S, Morgner U, Meinhardt-Wollweber M, Rahlves M, Roth B. Trimodal system for in vivo skin cancer screening with combined optical coherence tomography-Raman and colocalized optoacoustic measurements. J Biophotonics. 2018;11(6):e201700288.
43. Mazurenka M, Behrendt L, Meinhardt-Wollweber M, Morgner U, Roth B. Development of a combined OCT-Raman probe for the prospective clinical melanoma skin cancer screening. Rev Sci Instrum. 2017;88(10):105103.
44. Krasnikov I, Suhr C, Seteikin A, Meinhardt-Wollweber M, Roth B. Monte Carlo simulation of the influence of internal optical absorption on the external Raman signal for biological samples. J Opt Soc Am A. 2019;36:877–82.
45. Wang S, Zhao J, Lui H, He Q, Bai J, Zeng H. Monte Carlo simulation of in vivo Raman spectral measurements of human skin with a multi-layered tissue optical model. J Biophotonics. 2014;7(9):703–12.
46. Zeng H, MacAulay C, Mclean DI, Palcic B. Reconstruction of in vivo skin autofluorescence spectrum from microscopic properties by Monte Carlo simulation. J Photochem Photobiol B Biol. 1997;38:234–40.
47. Chen R, Huang Z, Lui H, Hamzavi I, Mclean DI, Xie S, Zeng H. Monte Carlo simulation of cutaneous reflectance and fluorescence measurements—the effect of melanin contents and localization. J Photochem Photobiol B Biol. 2007;86:219–26.
48. Wang S, Zhao J, Lui H, He Q, Zeng H. Monte Carlo simulation of near infrared autofluorescence measurements of in vivo skin. J Photochem Photobiol B Biol. 2011;105:183–9.
49. Wang S, Zhao J, Lui H, He Q, Zeng H. A modular Raman microspectroscopy system for biological tissue analysis. Spectroscopy. 2010;24:577–83.
50. Novikova T, Rehbinder J, Deby S, Haddad H, Vizet J, Pierangelo A, Validire P, Benali A, Gayet B, Teig B, Nazac A, Drévillon B, Moreau F, De Martino A. Multi-spectral Mueller matrix imaging polarimetry for studies of human tissues. In: Biomedical optics, OSA Technical Digest TTh3B, 2; 2016.
51. Qi J, Elson DS. Mueller polarimetric imaging for surgical and diagnostic applications: a review. J Biophotonics. 2017;10:950.
52. Antonelli M-R, Pierangelo A, Novikova T, Validire P, Benali A, Gayet B, De Martino A. Mueller matrix imaging of human colon tissue for cancer diagnostics: how Monte Carlo modeling can help in the interpretation of experimental data. Opt Express. 2010;18(10):10200–8.
53. Du E, He H, Zeng N, Sun M, Guo Y, Wu J, Liu S, Ma H. Mueller matrix polarimetry for differentiating characteristic features of cancerous tissues. J Biomed Opt. 2014;19(7):076013-1–8.
54. Lu S-Y, Chipman RA. Interpretation of Mueller matrices based on polar decomposition. J Opt Soc Am A. 1996;13(5):1106–13.
55. Agarwal N, Yoon J, Garcia-Caurel E, Novikova T, Vanel J-C, Pierangelo A, Bykov A, Popov A, Meglinski I, Ossikovski R. Spatial evolution of depolarization in homogeneous turbid media within the differential Mueller matrix formalism. Opt Lett. 2015;40:5634–7.
56. Doronin A, Macdonald C, Meglinski IV. Propagation of coherent polarized light in turbid highly scattering medium. J Biomed Opt. 2014;19(2):025005.
57. Kuzmin V, Meglinski I. Coherent effects of multiple scattering for scalar and electromagnetic fields: Monte-Carlo simulation and Milne-like solutions. Opt Commun. 2007;273(2):307–10.
58. Nieuwenhuizen T, Luck J. Skin layer of diffusive media. Phys Rev E. 1993;48(1):569–88.
59. Amic E, Luck J, Nieuwenhuizen TM. Anisotropic multiple scattering in diffusive media. J Phys A Math Gen. 1996;29(16):4915–55.
60. Kuzmin V. The Milne problem solution for the temporal correlation function of an electromagnetic field. Opt Spectrosc. 2002;93(3):439–48.
61. Kuzmin V, Aksenova E. A generalized Milne solution for the correlation effects of multiple light scattering with polarization. J Exp Theor Phys. 2003;96(5):816–31.
62. Kirillin M, Meglinski I, Kuzmin V, Sergeeva E, Myllylä R. Simulation of optical coherence tomography images by Monte Carlo modeling based on polarization vector approach. Opt Express. 2010;18(21):21714–24.
63. Doronin A, Radosevich AJ, Backman V, Meglinski I. Comparison of two Monte Carlo models of propagation of coherent polarized light in turbid scattering media. Proc SPIE. 2014;8952:89520F.
64. Doronin A, Radosevich AJ, Backman V, Meglinski I. Two electric field Monte Carlo models of coherent backscattering of polarized light. J Opt Soc Am A. 2014;31(11):2394–400.
65. Meglinski I, Kirillin M, Kuzmin V, Myllylä R. Simulation of polarization-sensitive optical coherence tomography images by a Monte Carlo method. Opt Lett. 2008;33(14):1581–3.
66. Doronin A, Vera N, Staforelli JP, Coelho P, Meglinski I. Propagation of cylindrical vector laser beams in turbid tissue-like scattering media. Photonics. 2019;6(2):56.
67. Wollweber M, Roth B. Raman sensing and its multimodal combination with optoacoustics and OCT for applications in the life sciences. Sensors. 2019;19(10):2387.